Simulation and experimental validation of the effect of superheat on macrosegregation in large-size steel ingots

C. Zhang, M. Jahazi and R. Tremblay

Simulation and experimental validation of the effect of superheat on macrosegregation in large-size steel ingots

C. Zhang[1] ✉, M. Jahazi[1], R. Tremblay[2]

[1] Mechanical Engineering Department, École de Technologie Supérieure, 1100 Rue Notre-Dame Ouest, Montreal, Quebec H3C1K3, Canada

[1] Mechanical Engineering Department, École de Technologie Supérieure, 1100 Notre-Dame Street West, Montreal, Quebec, H3C 1K3, Canada
[2] Finkl Steel-Sorel, 100 McCarthy Street, Saint-Joseph-de-Sorel, Quebec, J3R 3M8, Canada

C. Zhang
e-mail: chunping.zhang.1@gmail.com
tel.: 001-5143968800-7868
fax: 001-5143968530

M. Jahazi
e-mail: Mohammad.Jahazi@etsmtl.ca
tel.: 001-5143968974
fax: 001-5143967536

R. Tremblay
e-mail: rtremblay@finkl.com
tel.: 001-4507464030
fax: 001-4507464092

Abstract

A 3D model was employed to study the effect of melt initial superheat on the macrosegregation formation using FE modeling and experimentation methods. The casting process of three ingots with the initial melt superheats of 75°C, 65°C and 55°C were simulated. The three cases represented three variables encountered in industry during casting of large size ingots. For the above three studied cases, all other casting conditions were kept the same. Results showed that the variation of initial melt superheat gave rise to changes in temperature pattern, liquid flow field, solidification speed, and thermomechanical contraction. Under the combined actions of all these changes, lower superheat tended to alleviate the segregation intensity in the upper part of the ingot body, in the hot-top, and in the solute-rich bands between the ingot centerline and periphery. The beneficial effect of lower superheat on alleviation of segregation severity was confirmed by experimental chemical measurement results. The results were analyzed in terms of heat and mass transfer theories and allow for a better understanding of the underlying mechanisms responsible for the occurrence of macrosegregation in ingot casting process. The findings should be helpful for the casting process design of a given ingot of high value-added steels or other alloys.

Key words: Finite Element modeling · Large-size ingot · Steel · Superheat · Solidification · Macrosegregation

1 Introduction

During casting in industry, non-equilibrium conditions prevail, resulting in chemical heterogeneities on the scale of the entire ingot and the formation of so-called macrosegregation [1]. Macrosegregation of solutes is one of the most significant casting defects in large size ingots [2], as it is difficult to alleviate and completely remove using any subsequent practical heat treatment and mechanical process [3, 4].

In order to achieve high quality large-size cast ingots, a better understanding of the influence of chemical composition and process parameters is needed in order to be able to take measures for minimizing the extent

and intensity of macrosegregation. The measures commonly taken include control of chemical compositions (reduction of Mn and Si contents) [5], improvement in mold geometry [6, 7], optimisation of casting process (control of melt temperature, mold preheating temperature, filling rate) [8, 9], employment of engineering solution (intensive rapid cooling, mechanical vibration and electromagnetic stirring) [10, 11], and application of multipouring technique (sequential pouring of molten steel from multiple ladles with different concentrations of alloying elements) [12]. Among the above strategies, superheat control is one of the simplest methods to implement. Superheat is excess of the casting temperature above the liquidus [13]. Despite numerous studies on the impact of superheat on macrosegregation, the function of superheat is, however, still unclear or even controversial, and far from conclusive.

Liu et al. numerically studied the formation mechanism of macrosegregation in a 3.3t steel ingot and ascribed the reduced height of bottom negative segregation cone with higher superheat to the variations of flow field [14]. Pikkarainen et al. investigated the continuous casting of low-alloyed steel, and found that a higher superheat caused smaller segregation in the central fine equiaxed dendritic structures, while a low superheat brought about negative segregation due to sedimentation of globulites and higher segregation in the central coarse globular structures [8]. Zhong et al. studied the permanent mold casting of a ferrite-based alloy, and pointed out that with superheat increasing, coarser equiaxed dendritic grains formed and secondary dendritic arm spacing increased, but carbon segregation became less intense [15]. EI-Bealy and Hammouda modeled the solidification of Al-Cu ingots, and reported that with increasing superheat, the magnitude of convection velocities increased, the grain size of equiaxed crystals decreased and macrosegregation decreased [16].

In contrast, Mäkinen and Uoti declared that low superheat favored an equiaxed structure, which can minimize the severity of centerline macrosegregation in continuous casting of low-alloyed copper billets [17]. Sun et al. reported that a lower melt superheat and a higher nucleation density decreased the severity of macrosegregation by weakening the flotation of grains [18]. Guan et al. demonstrated that V-shaped segregation decreased with decreasing superheat in continuous casting blooms [19]. Choudhary and Ganguly observed that low superheat favored the surviving of equiaxed crystals, which ejected solutes uniformly within the mushy zone, resulting in a reduction in segregation [20]. Yadav et al. simulated the filling and solidification process of side-cooled Pb-Sn alloy, and pointed out that when superheat was low, considerable amount of solidification occurred during filling of the cavity, causing some positive segregation near the wall, and then negative segregation subsequently formed due to the slowing-down of the solidification rate resulting from the continuous supply of hotter melt by convection [21]. Eskin et al. performed experimental and numerical investigations of the direct-chill (DC) casting of an Al-Cu alloy, and observed coarsened structure coarsening, increased probability of bleed-outs, increased severity of subsurface segregation, and unaffected macrosegregation in the rest of the billet with increased casting temperature [22].

Based on the above conflicting findings on the effect of melt superheat on macrosegregation, we are urged to turn to experimental and simulation investigations for an answer. The objective of the present study is to investigate the impact of melt initial superheat on macrosegregation in a production scale ingot (40 metric ton (MT)) of a low-alloy high strength steel. A 3D two phase (liquid-solid) multiscale thermomechanical solidification model was used and the simulations were performed in the finite element code Thercast® [23]. The mold filling and solidification processes of 3 ingots with different melt superheats were simulated. The evolution of solute transport as well as its associated phenomena throughout the filling and cooling stages, including the bulk liquid flows, the thermal/solutal convection and the thermomechanical deformation of the phases were all investigated. The dimensional tolerance and surface finish, however, were not examined due to their less importance compared to the global macrosegregation profile for the quality of the ingot and also due to the later performance of reheating and forging on the as-cast ingot in industry." The predictions were compared with the chemical measurements on two experimentally obtained 40MT steel as-cast ingots. The findings will contribute to a better understanding of the macrosegregation formation mechanisms in ingot casting process. They could also be used in industry to improve the quality of large-sized ingot production and the productivity of high value-added steels or other alloys, which are prone to macrosegregation.

2 Model establishment and experimental process

The used model is a casting system, as shown in Figure 1a, composed of a cylindrical ingot (250cm in height and 150cm in average diameter) in big-end-up cast iron mold with an above hot-top 70cm in height. The hot-top part is lined inside with insulating refractory tiles, and an exothermic refractory board is laid above on the melt top. 3D linear tetrahedral elements, with an average grid of 35mm, were used for the spatial discretization of the part and mold components.

The chemical composition of the steel in study is given in Table 1. For the simulations, the liquid steel is bottom poured into the mold at different temperatures with a filling time of 30min. Three superheats of 75°C (pouring melt temperature of 1570°C), 65°C (pouring melt temperature of 1560°C) and 55°C (pouring melt temperature of 1550°C) were investigated. The three simulated superheat cases represented three variables encountered in industry for casting large-size ingots. The three simulated cases were identified, in the rest of this manuscript, as 75M (for superheat of 75°C), 65M (for superheat of 65°C), 55M (for superheat of 55°C), reflecting their respective superheat.

Table 1 Nominal composition of the studied steel (wt.%)

C	Si	Mn	S	Cr	Mo	P	Ni	Fe
0.36	0.4	0.85	0.0023	1.82	0.45	0.01	0.16	Balance

The predicted carbon segregation ratio profiles were compared with the chemical measurements from two experimental obtained 40MT steel ingots. One is the 75E (cast at initial melt superheat of 75°C, pouring melt temperature of 1570°C), and the other is 62E (cast at the initial melt superheat of 62°C, pouring melt temperature of 1557°C). The compositional determination for the experimentally-obtained ingots was conducted on $4.5 \times 6.5 cm^2$ small samples, using Thermo Scientific ARL^{TM} 4460 mass spectrometer. Segregation ratio of carbon (for both experiment measurements and simulation predictions) on each sampling, R_C, was determined based on the relation: $R_C = (\omega_C - \omega_{0,C}) / \omega_{0,C}$, where ω_C is the local carbon concentration and $\omega_{0,C}$ is its nominal concentration value [24]. A positive/negative R_C value corresponds to positive/negative segregation. For all the above simulated and experimentally obtained cases, all casting conditions were kept the same expect for initial melt superheat. The material parameters for the FE simulations were all from Zhang et al. [25].

3 Results and discussions

3.1 Macrosegregation patterns and verification

Figure 1 reports the evolution of macrosegregation pattern of carbon in the casting process for the three initial superheat cases 75M, 65M and 55M. As featured in the figure, different initial melt superheat produced varied large-scale compositional distribution from the mold pouring moment till the end of solidification. At the end of the filling operation, as compared among Figures 1a, 1e and 1i, in the lowest superheat case (55M with 55°C superheat), more first segregated particles (red and blue spots) formed in a larger region. As the solidification proceeded, as reported in Figures 1b, 1f and 1j, the weakest accumulation of solutes occurred in the lowest initial superheat case (i.e. 55M). This feature was reflected in the upper section of the ingot, in the hot-top and in the mid-radius solute-enriched bands. Such trend was maintained until the completion of solidification, as seen in the rest figures of Figure 1. The predicted smaller extent of segregation at lower superheat is in agreement with the findings reported by Mäkinen and Uoti [17], Sun et al. [18], as well as Choudhary and Ganguly [19].

The comparison among the three cases on the final segregation ratio profiles of carbon along the ingot central axis was plotted in Figure 2a. It can be seen that with the decrease of the superheat by 10°C (from the case 75M to 65M, or from 65M to 55M), the segregation ratio intensity was generally alleviated by about 9% in the upper half of the ingot body and in the hot-top. Similar effect of lower superheat on alleviation of macrosegregation was also observed in the horizontal direction on the section located 30cm below the hot-top/ingot body separation interface, as presented in Figure 2b. The segregation ratio intensity inside the mid-radius positive-segregated bands in 55M was found to be, in average, 10% and 20% lower than that in 65M and 55M, respectively.
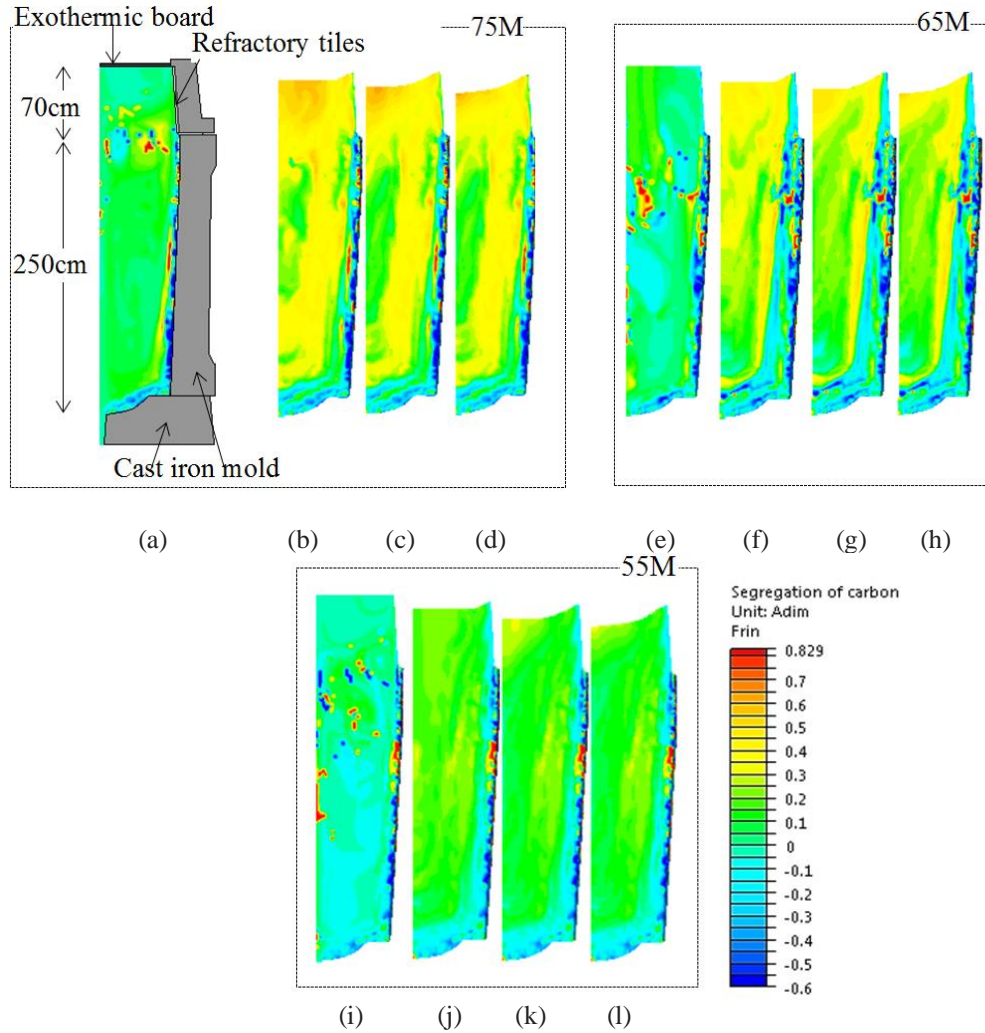
4

Fig. 1 Segregation ratio patterns of carbon during the casting process predicted by 75M (upper left group), 65M (upper right group), and 55M (lower group) at times of **a e i** 0.5h (end of filling). **b f j** 5.5h. **c g k** 10.5h. **d h l** End of solidification

The carbon segregation profiles of experimentally cast ingots 75E (75°C initial superheat) and 62E (62°C initial superheat) were also reported in Figure 2. In Figure 2a, the centerline carbon segregation distribution curve from lower superheat case (i.e. 62E) was located closer to the zero-segregation line than that from 75E, demonstrating the decrease of the segregation intensity when initial melt superheat was decreased. Particularly, the measured centerline carbon profile from 62E lied between the predicted profile from 65M (under 65°C superheat condition) and that from 55M (with 55°C initial superheat), yet closer to that from 65M. The above features were also remarked in the regions in the vicinity of the ingot axis in Figure 2b. The good agreement of the chemical predictions with the experimental measurements, in both vertical and radial directions, verified the beneficial effect of the decreasing initial superheat on the decrease of macrosegregation intensity.

Furthermore, in Figure 2a, the experimental results showed that the segregation intensity in the top center of the hot-top increased with lowering the melt superheat, which was in contrast to the simulation predictions. The above observations are in agreement with the findings of Lesoult [26], who reported the underestimation of positive segregation severity at the top of the ingot and the resulting overestimation of solutes concentrations at the bottom of the ingot due to the neglecting of the sedimentation of free equiaxed grains and solid fragments in modeling.
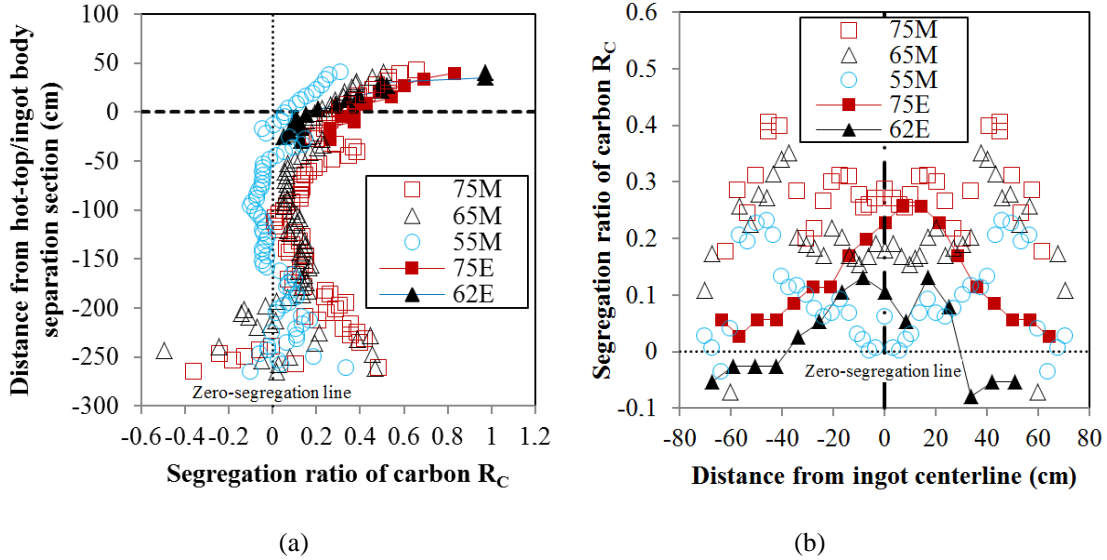
Fig. 2 Predicted and measured segregation ratio profiles of carbon at the end of solidification. **a** In the vertical direction along the ingot centerline. **b** In the horizontal direction along the section at 30cm below the hot-top/ingot body separation interface

In addition, in Figure 2b, the measured positive segregation intensities in the regions between the ingot centerline and the periphery were lower than the predicted ones, which could be due to the measurement sampling method (a compilation of over 250 measurements on $4.5 \times 6.5 cm^2$ small samples). New experimental measurements with a sampling density of $0.9 \times 0.9 cm^2$ revealed an 8% decrease in segregation intensity inside the solute-rich bands with the decrease of the initial melt superheat from 75°C (75E, as seen in Figures 3a and 3b) to 62°C (62E, Figures 3c and 3d). These experimental results confirmed the above-mentioned predictive reasonability that the segregation inside the mid-radius solute-rich bands was alleviated with the initial melt superheat decreased.
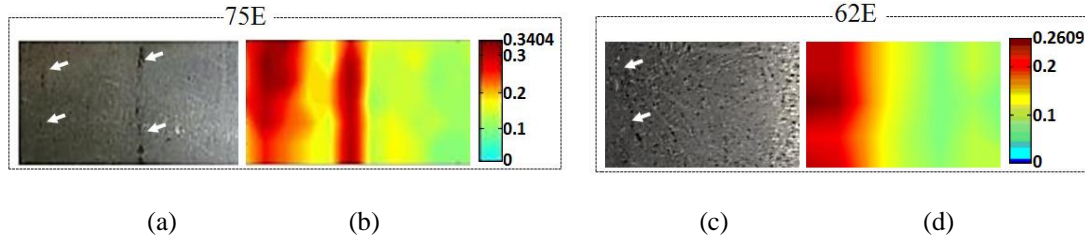

Fig. 3 Characterizations in mid-radius position on the section 30cm below the hot-top/ingot body interface for the experimentally obtained ingots 75E and 62E. **a c** Macrograph with solute-rich black bands illustrated with white arrows. **b d** Segregation ratio pattern of carbon measured using mass spectrometer with sampling density of $0.9 \times 0.9 cm^2$

Based on the above results, it can be said that lower initial melt superheat helped to decrease the macrosegregation severity in the upper part of the ingot body, in the centerline and in the solute-enriched bands between the ingot centerline and surface. This finding indicates that the varied solidification behavior in the ingot induced by different initial superheat exerts a significant impact on the compositional distributions, as will be discussed in the following sections.

3.2 Temperature gradient

The predicted temperature fields at times of 0.5h (end of filling), 5.5h and 10.5h after pouring are given in the left half of each pattern in Figure 4. At the end of the filling phase (Figures 4a, 4d and 4g), at the lowest

6

initial melt temperature condition (55M), the 1550ºC isotherm became longer and more inclined towards the hot-top upper skin region and smaller liquid area (the red regions above the 1550ºC isotherm) was left. These features indicate that the acceleration of energy loss was induced by decreasing initial melt temperature, which could be resulted from the less thermal energy provided by the less hot melt.
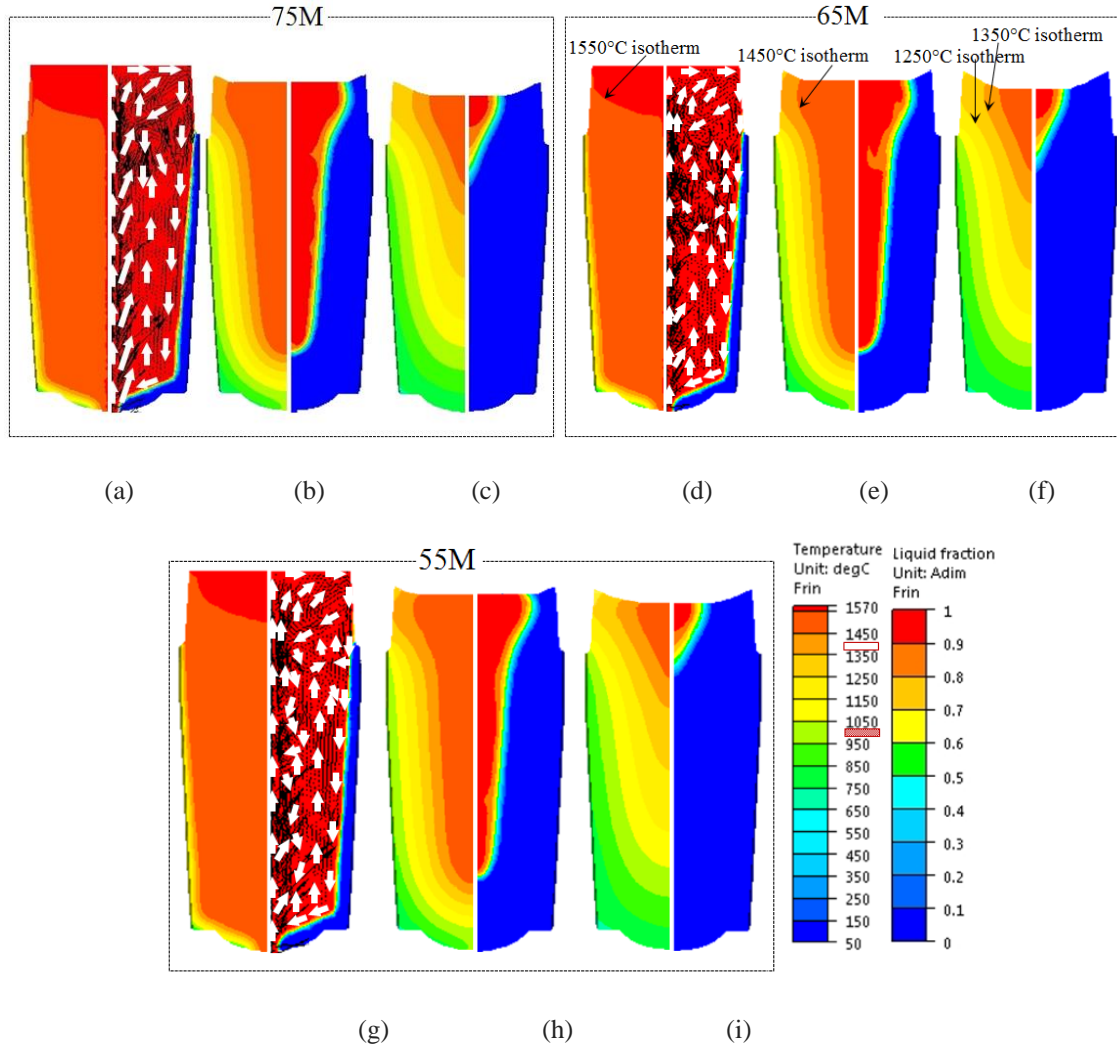

(a)   (b)   (c)   (d)   (e)   (f)

(g)   (h)   (i)

Fig. 4 Temperature field (left figures) and liquid fraction patterns combined with velocity vectors (right figures) predicted by 75M, 65M and 55M at times of **a d g** 0.5h (end of filling). **b e h** 5.5h. **c f i** 10.5h after pouring

In the intermediate and later solidification stages, as displayed in Figures 4b, 4c, 4e, 4f and compared with Figures 4h, 4i, the distances between adjacent isotherms, whether vertically or radially, tended to be larger under lower superheat condition. For instance, at 5.5h, in the case with smaller superheat, the 1450ºC isotherm moved farther away from the 1350ºC one next to the hot-top wall side, as compared among Figures 4b, 4e and 4h. Similar tendency was also observed at 10.5h between 1350ºC and 1250ºC isotherms (Figures 4c, 4f and 4i). The above characteristics are indicative of the production of smaller temperature gradient when lowering initial melt temperature.

Figure 5 plots the displacements of 1450ºC and 1050ºC isotherms (as identified in the Figure 4 color bar) as a function of time during the solidification process, for the three studied cases. It can be seen that for the lower superheat case, in the radial direction on the hot-top/ingot body separation section (Figure 5a), the two investigated isotherms were located closer to the ingot axis; in the vertical direction along the ingot centerline

7

(Figure 5b), they lay farther from the ingot bottom. These observations confirmed the above-mentioned acceleration of energy loss under lower superheat condition. Furthermore, it was noted that in the lowest superheat case (55M), the distance between the two examined isotherms, both radially and vertically, kept larger. Quantitative examination revealed that 10°C superheat decrease brought about 2cm enlargement in the two isothermal curves distance in the radial direction on the hot-top/ingot body separation section (Figure 6a) and about 3.2cm broadening in the vertical direction along the ingot centerline (Figure 6b). The quantitative results evidenced the creation of smaller thermal gradient when lower initial melt temperatures were used.
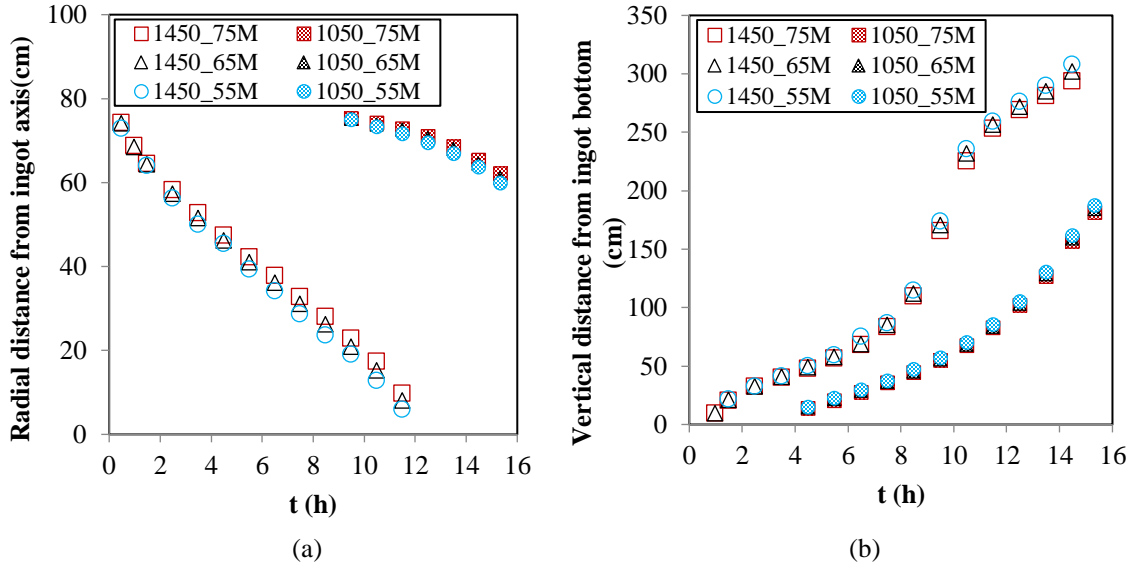

Fig. 5 Movement of 1450°C and 1050°C isotherms with time. **a** In the radial direction. **b** In the vertical direction
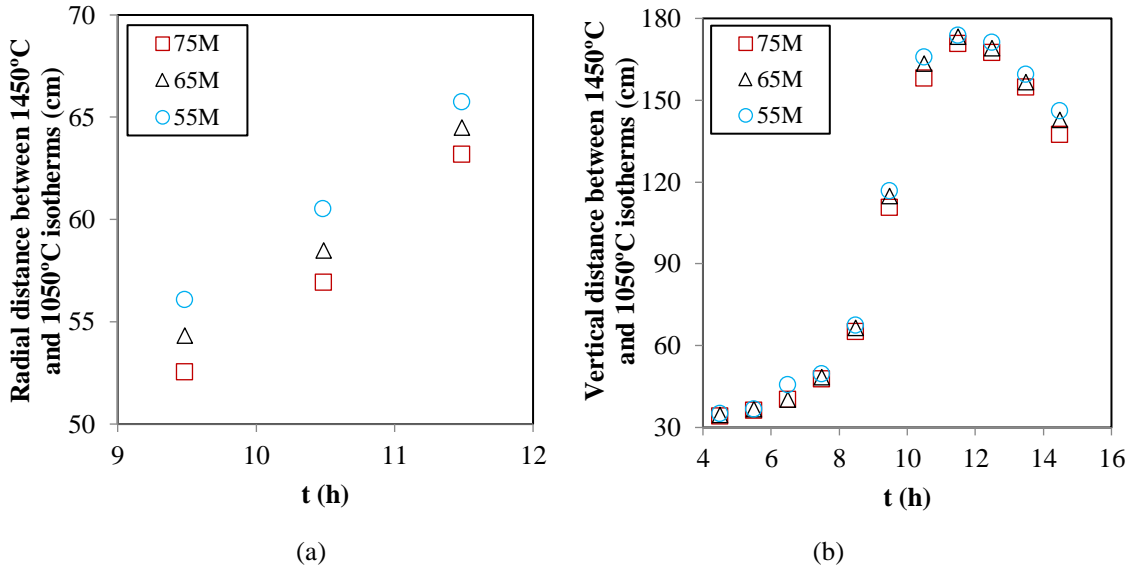

Fig. 6 Distance between 1450°C and 1050°C isotherms with time. **a** In the radial direction. **b** in the vertical direction

The smaller temperature gradient in the case with lower initial melt superheat should be the root cause for their milder segregation in the steel casting, as observed in Figures 1 and 2. Based on the reports from

others [27-29], smaller thermal gradient coexists with decreased density gradient, which leads to delayed development of solutal convection, inhibiting the accumulation of solutes in the solidification process.

3.3 Liquid flow and solidification speed

Liquid fraction field combined with velocity vectors were reported in the right half of the patterns in Figure 4. As seen in Figures 4a, 4d and 4g, clockwise and counter-clockwise cells coexisted in the bulk liquid in the intermediate (65M) and lowest superheat cases (55M). These features were in contrast to 75M, in which only clockwise vortex existed in the upper part where the first solid particles started to form in the melt. More inversion of clockwise movement was observed inside the ingot body in lower superheat case, counteracting the orderly liquid bulk flow. The occurrence and multiplication of counter-clockwise streams in the early solidification stage could arise from the earlier dominance of natural convection flow, induced by the earlier triggering and quicker development of radial temperature gradient in lower initial superheat cases, as observed and discussed in section 3.1. The greater destabilization of the bulk liquid flow could be the origin of first solid particles scattering in wider regions at the initial period of solidification in the simulations with lower superheat.

Further analyses on the liquid fraction evolution revealed that thicker solid shell was always observed next to the chill wall in the hot-top at lower superheat condition, as also reported by Yadav et al. [13]. In addition, at 10.5h after pouring (Figures 4c, 4f and 4i), less liquid (red zone areas) was left in the calculations with smaller initial superheat. These features suggested that smaller initial melt superheat increased the solidification rate and quickened up the solidification process.

The solidification acceleration caused by the reduction of superheat was also revealed by the solidification time analysis results, as presented in Figure 7. It was predicted that smaller initial superheat advanced the completion of the solidification by a few seconds in the first solidified region at the bottom corner of the ingot. The predicted total solidification time for 55M (53103s with 55°C as the initial melt superheat) was 11min and 22min, respectively, shorter than the time needed for 65M (53757s with 65°C as the initial superheat) and 75M (54428s with 75°C as the initial superheat).
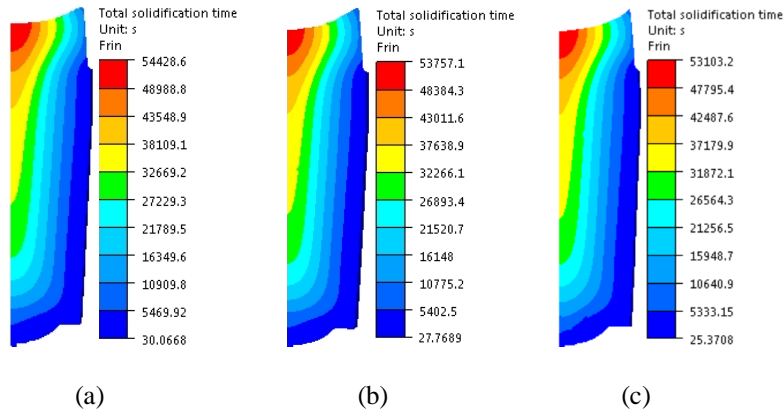

Fig. 7 Total solidification times predicted by **a** 75M. **b** 65M. **c** 55M

The faster solidification process in lower initial superheat case could be associated with its larger casting volume contraction, as reported in Figure 8. Figure 8a plotted the evolution of lateral air gap formation and the top shrinkage during the casting process on four selected points (as illustrated on the upper right corner of Figure 8a). The radial displacements on Point1 (at the ingot bottom skin in blue), Point2 (at the hot-top/ingot body junction skin in green), Point3 (at the top skin of hot-top in red), and the vertical displacement on Point4 (at the top center of the hot-top in black), were monitored during the whole filling and solidification processes. As seen in the figure, lower initial superheat created earlier creation of the radial air gap on Point3 and larger air gap size on Points 2 and 3, indicating wider air gap from the bottom to the top along the casting

height. When it comes to the top shrinkage examination on Point4, lower initial superheat was in line with quicker development of top contraction and larger shrinkage degree.

Figure 8b quantified the radial and vertical shrinkage differences on the same examined point among the three studied cases. It can be noted that at 16h, the difference in the radial air gap width on Point3 between 65M and 75M was 0.15cm, while it got to 0.33cm between 55M and 75M on the same point. The variation in the vertical shrinkage on Point4 between 65M and 75M and that between 55M and 75M reached 1.3cm and 2.8cm, respectively.
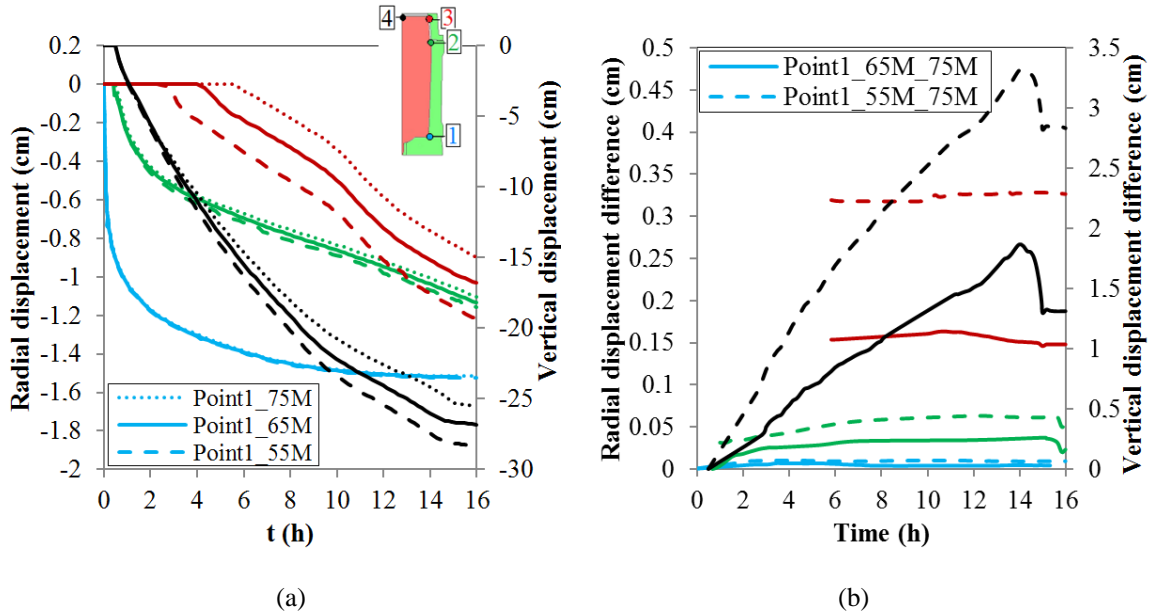

(a)   (b)

Fig. 8 Examination of ingot volume contraction in the solidification process of three superheat cases. **a** Predicted time-dependent displacements of Points 1-3 in the radial direction and Point4 in the axial direction. **b** Displacement differences between 65M/55M and 75M on Points 1-3 in the radial direction and Point4 in the axial direction

The above analyses of the time-dependent radial and vertical displacements of the casting skin presented that the reduction of the initial superheat led to the increase of the air gap and top shrinkage sizes. The combination of the larger shrinkage at the top of the casting and the wider radial air gap detached the casting away from the top and the mold walls, leading to a bigger volume reduction. This higher volume reduction in the lower superheat case should be the origin of its higher solidification speed and faster solidification process.

The milder segregation in lower superheat cases could find its origin in three aspects, as discussed above: 1) the weaker solutal convection induced by the lower density gradient resulting from the lower temperature gradient in the bulk liquid; 2) the more disordered thermal convection flow, which could impede the directed distribution of the rejected solutes; and 3) the accelerated solidification in the casting process due to greater ingot volume reduction, which could result in less time available for solutes to transport. The combined action of the three sources weakened the accumulation of species, resulting in minimized segregation intensity.

4 Conclusion

In the present work, the effect of melt initial superheat on the macrosegregation pattern of a 40MT steel ingot was investigated. A thermomechanic model considering both convection and solidification shrinkage was developed. The whole filling and casting processes of three ingots with different superheats were simulated. The evolution of macrosegregation patterns, as well as the associated phenomena, including the evolution of the temperature gradient, solidification speed, top shrinkage, air gap formation, and fluid flow were all

analyzed. The following conclusions can be drawn from the experimental and simulation results:

1) Lower superheat tended to advance the initiation and quicken up the development of temperature gradient in the early solidification stage, and also decrease the temperature gradient, both radially and vertically, in the later solidification phase.
2) Lower superheat led to greater top shrinkage and lateral air gap size, which resulted in larger volume reduction and less solidification time.
3) Lower superheat gave rise to earlier dominance of thermal convection, weaker solute convection, and alleviated segregation in the upper part of the ingot body, in the hot-top, and in the mid-radius solute-rich bands.

The established model and the predictions have been verified with the chemical experimental measurements. The findings are expected to contribute to a better understanding of the macrosegregation formation mechanisms in ingot casting process. The decrease of the superheat should be a practical method for the casting process design of a given ingot of high value-added steels or other alloys.

References

1. Pickering EJ (2013) Macrosegregation in Steel Ingots: The applicability of modelling and characterisation techniques. ISIJ Int 53:935-949. https://doi.org/10.2355/isijinternational.53.935
2. Becker WT, Shipley RJ (2002) Failures related to metalworking in failure analysis and prevention. ASM Handbooks. Vol. 11, ASM International, Materials Park, OH. USA; 5-81. ISBN: 978-0-87170-704-8
3. Loucif A, Ben Fredj E, Harris N, Shahriari D, Jahazi M, Lapierre-Boire LP (2018) Evolution of A-type macrosegregation in large size steel ingot after multistep forging and heat treatment. Metall Mater Trans B 49:1046-1055. https://doi.org/10.1007/s11663-018-1255-2
4. Scarabello D, Ghiotti A, Bruschi S (2013) FE modelling of large ingot hot forging. Int J Mater Form 3, Supp 1:335-338. https://doi.org/10.1007/s12289-010-0775-3
5. Suzuki K, Taniguchi K (1981) The mechanism of reducing "A" segregates in steels ingots. T ISIJ 21: 235-242.
6. Dub VS, Romashkin AN, Mal'ginow AN, Ivanov IA, Tolstykh DS (2014) Effect of the geometry of an ingot on its chemical heterogeneity. Part I. Metallurgist 57:987-995. https://doi.org/10.1007/s11015-014-9834-1
7. Lesoult G (2005) Macrosegregation in steel strands and ingots: characterization, formation and consequences. Mater Sci and Eng A 413-414: 19-29. https://doi.org/10.1016/j.msea.2005.08.203
8. Pikkarainen T, Vuorenmaa V, Rentola I, Leinonen M, Porter D (2016) Effect of superheat on macrostructure and macrosegregation in continuous cast low-alloy steel slabs. 4th International Conference on Advances in Solidification Processes (ICASP-4) IOP Publishing IOP Conf Series: Materials Science and Engineering 117:012064. https://doi.org/10.1088/1757-899X/117/1/012064
9. Zhang C, Loucif A, Jahazi M, Tremblay R, Lapierre LP (2018) On the effect of filling rate on positive macrosegregation patterns in large-size cast steel ingots. Appl Sci 8: 1878. https://doi.org/10.3390/app8101878
10. Galkin AN, Zyuban NA, Rutskii DV, Gamanyuk SB, Puzikov AY, Firsenko VV (2013) Effect of chilling of the top part of a steel ingot on the conditions of its crystallization and the quality of forgings obtained from it. Metallurgist 57: 199-206. https://doi.org/10.1007/s11015-013-9713-1
11. Zhang B, Cui J, Lu G (2003) Effect of low-frequency magnetic field on macrosegregation of continuous casting aluminum alloys. Mater Lett 57:1707-1711. https://doi.org/10.1016/S0167-577X(02)01055-8
12. Tu WT, Shen HF, Liu BC (2015) Modelling of macrosegregation in a 231-ton steel ingot with multi-pouring Process. Mater Rese Innov 19:S59-S63. https://doi.org/10.1179/1432891715Z.0000000001517
13. Campbell J (2011) Complete casting handbook, metal casting processes, metallurgy, techniques and design. 2nd ed. Butterworth-Heinemann, Elsevier ltd., USA
14. Liu DR, Kang XH, Fu PX, Li DZ (2011) Modeling of macrosegregation in steel ingot: influence of mold shape and melt superheat. Kovove Mater 49:143-153. https://doi.org/10.4149/km-2011-2-143

15. Zhong H, Tan Y, Li H, Mao X, Zhai Q (2012) The effect of high superheat on the solidification structure and carbon segregation of ferrite-based alloy. Supplemental proceedings: Materials Processing and Interfaces TMS (the Minerals, Metals & Materials Society) 1:215-220. ttps://doi.org/10.1002/9781118356074.ch29

16. EI-Bealy MO, Hammouda RM (2007) On the mechanism of natural convection and equiaxed structure during dendritic solidification processes. Steel Research int 78:602-611. https://doi.org/10.1002/srin.200706255

17. Mäkinen M, Uoti M (2006) The effect of superheat on micro- and macrosegregation and crack formation in the continuous casting of low-alloyed copper. Mater Sci Forum 508:549-554. https://doi.org/10.4028/www.scientific.net/MSF.508.549

18. Sun QY, Liu DR, Zhang JJ, Wang LP, Guo EJ (2016) Numerical simulation of macrosegregation with grain motion during solidification of Mg-4wt.%Y alloy. Mod Phys Lett B 30:1450417. https://doi.org/10.1142/S0217984916504170

19. Guan R, Ji C, Zhu M, Deng S (2018) Numerical simulation of V-shaped segregation in continuous casting blooms based on a microsegregation model. Metall Mater Trans B 49:2571-2583. https://doi.org/10.1007/s11663-018-1352-2

20. Choudhary S, Ganguly S (2007) Morphology and segregation in continuously cast high carbon. ISIJ Int 47:1759-1766. https://doi.org/10.2355/isijinternational.47.1759

21. Yadav A, Pathak N, Kumar A, Sarkar S (2009) Effects of the filling process on the evolution of the mushy zone and macrosegregation in alloy casting. Model Simul Mater Sci Eng 17:035006 https://doi.org/10.1088/0965-0393/17/3/035006

22. Eskin DG, VSavran VI, Katgerman L (2005) Effects of melt temperature and casting speed on the structure and defect formation during direct-chill casting of an Al-Cu alloy. Metall Mater Trans A 36:1965-1976. https://doi.org/10.1007/s11661-005-0059-6

23. TherCast 8.2®, Transvalor, S.A., Cedex, France

24. Duan Z, Tu W, Shen B, Shen H, Liu B (2016) Experimental measurements for numerical simulation of macrosegregation in a 36-ton steel ingot. Metall Mater Trans A 47:3597–3605. https://doi.org/10.1007/s11661-016-3531-6

25. Zhang C, Shahriari D, Loucif A, Melkonyan H, Jahazi M (2018) Influence of thermomechanical shrinkage on macrosegregation during solidification of a large-sized high-strength steel ingot. Int J Adv Manuf Technol 99:3035-3048. https://doi.org/10.1007/s11661-016-3531-6

26. Lesoult G (2005) Macrosgregation in steel strands and ingots: Characterisation, formation and consequents. Mater Sci Eng A 413-414:19-29. https://doi.org/10.1016/j.msea.2005.08.203

27. Zhang C, Bao Y, Wang M (2016) Influence of casting parameters on shrinkage porosity of a 19 ton steel ingot. Metall Ital 1:37-44

28. Hachani L, aadi B, Wang XD, Nouri A, Zaidat K (2012) Experimental analysis of the solidification of Sn–3 wt. % Pb alloy under natural convection. Intl J Heat Mass Transf 55:1986-1996. https://doi.org/10.1016/j.ijheatmasstransfer.2011.11.054

29. Liu SF, Liu LY, Kang LG (2008) Refinement role of electromagnetic stirring and strontium in AZ91 magnesium alloy. J Alloys Compd 450:546-550. https://doi.org/10.1016/j.jallcom.2007.07.053